J. Fluid Mech. (1995), *vol.* 302, *pp.* 45–63

The motion of a droplet subjected to linear shear flow including the presence of a plane wall

By W. S. J. UIJTTEWAAL† AND E. J. NIJHOF
Department of Medical and Physiological Physics, University of Utrecht, The Netherlands

(Received 14 December 1992 and in revised form 26 May 1995)

A fluid droplet subjected to shear flow deforms and rotates in the flow. In the presence of a wall the droplet migrates with respect to a material element in the undisturbed flow field. Neglecting fluid inertia, the Stokes problem for the droplet is solved using a boundary integral technique. It is shown how the time-dependent deformation, orientation, circulation and stability of a droplet are related to the capillary number and to the ratio of medium and droplet viscosity. The migration velocities are calculated in the directions parallel and perpendicular to the wall, and compared with theoretical models and experiments. The results reveal some of the shortcomings of existing models although not all discrepancies between our calculations and known experiments could be clarified.

1. Introduction

The dynamics of droplets and bubbles under shear conditions are of great importance in understanding the rheology of emulsions and the motions of droplet-like particles like biological cells. Following the work of Taylor (1932, 1934) a number of authors have dealt with this subject which has resulted in a large number of publications on experimental as well as theoretical research as reviewed by Rallison (1984). Most of the experimental work deals with the deformation and orientation of a fluid droplet either in a linear shear flow or in a hyperbolic flow (Rumscheidt & Mason 1961*a*; Torza, Cox & Mason 1972; de Bruin 1989). Rumscheidt & Mason (1961*a*, *b*) demonstrated the dramatic effects of tiny amounts of surface-active agents, often present in experiments as impurities, on the internal circulation of the droplet. It is therefore important to know whether the discrepancies found between experiments and analytical models (Torza *et al.* 1972; Rallison 1980), are due to the limitations of the models or to the imperfections in the experiments.

Experiments on the lateral motion of fluid droplets in shear flow near a boundary are difficult to perform as described in e.g. Goldsmith & Mason (1962), Karnis & Mason (1967), Chan & Leal (1981) and recently Smart & Leighton (1991). Although a lot of theoretical work has been done on the subject of droplet deformation (Cox 1969; Chan & Leal 1979; Chaffey, Brenner & Mason 1965; Barthès-Biesel & Acrivos 1973), the known analytical theories are only valid over a limited range of the governing parameters concerning deformation, orientation and time scale (Rallison 1980). The models describing lateral migration are all based on these deformation theories of limited application.

† Present address: Laboratory for Aero- and Hydrodynamics, Delft University of Technology, Rotterdamseweg 145, 2628 AL Delft, The Netherlands.

In order to explore the limitations of the analytical models on droplet deformation, a number of authors, starting with Youngren & Acrivos (1975), exploited the boundary integral technique in combination with numerical methods of solution. As yet the problems analysed numerically concern geometries with sufficient symmetry to reduce the calculations to one dimension. The only exceptions are Rallison (1981) and de Bruin (1989) who studied the deformation of a fluid droplet in unbounded, linear shear flow. Problems concerning the motion of a particle with respect to a plane boundary have been studied by Fischer (1987) who considered the inertia-induced lateral migration of a rigid sphere near a plane wall, and Pozrikidis (1992) who studied, among a variety of applications of the boundary integral method, the gravity-induced motion of a fluid droplet perpendicular to a wall in an otherwise quiescent fluid (Pozrikidis 1990). Very recently, Kennedy, Pozrikidis & Skalak (1994) presented their work on modelling droplet deformation and motion in simple shear flow, which shows similarities to the work presented in this paper, especially concerning unbounded flows. For the bounded case they give a few examples of lateral particle motion.

Our interest in this subject is mainly driven by the research on the motion of red blood cells in the vicinity of the vessel wall (Uijttewaal 1993). These cells are well known to deform in viscous shear flow and to migrate laterally away from a bounding wall, which has beneficial consequences for the circulatory system. In order to obtain insight into the deformation and migration mechanisms of such particles we started with the most simple approximation of a red blood cell in the form of a fluid droplet. In a previous paper (Uijttewaal, Nijhof & Heethaar 1993) we reported calculations on a fluid droplet near a plane wall undergoing shear flow by making use of the boundary integral method, and demonstrated the applicability of this technique in combination with a numerical method of solution. That work was, however, limited to the case where the viscosity of the fluid droplet equalled that of the suspending phase. Under these restrictions calculations were relatively easy to perform but comparison with experimental work was difficult owing to the lack of experimental data. In this paper we extend the model to include a droplet with viscosity different from the viscosity of the suspending phase. We are now able to investigate the effects of droplet viscosity and to make a more extensive comparison with experimental results and analytical models.

This paper is organized as follows. In §2 we will summarize the problem as it was stated in Uijttewaal *et al.* (1993) and give a description of the method of solution. The numerically calculated results for the configuration without a wall are given in §3. Data are presented on droplet deformation, orientation, internal circulation and transient motion, and they are compared with analytical models and experiments of other authors. Section 4 deals with the influence of a wall on the lateral and longitudinal motion with respect to the boundary and on the properties as given in §3.

2. Analysis of the problem

The definition of the problem under consideration is for the greater part similar to that of our previous paper (Uijttewaal *et al.* 1993), and those of other authors (Rallison 1981; de Bruin 1989; Pozrikidis 1990, 1992) and will therefore be treated only briefly.

A neutrally buoyant drop of viscosity η_i is suspended in a fluid of viscosity η_e, see figure 1. Both fluids are assumed to be Newtonian. The undeformed droplet with radius a is subjected to a linear shear flow G while positioned at a distance h from a plane wall. Owing to the applied flow field, the droplet will deform and orient itself with respect to the flow field. The interface of the droplet is maintained by the interfacial tension σ. The Reynolds number is assumed to be zero, leaving the problem

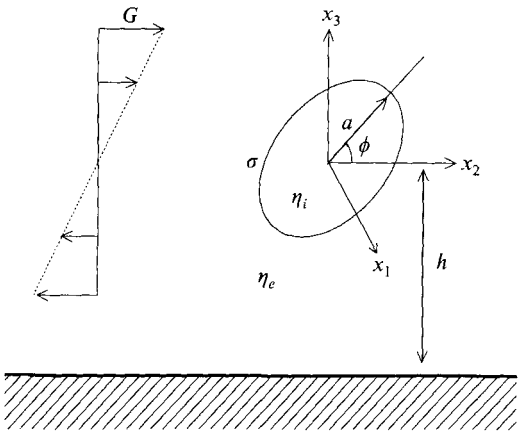

FIGURE 1. Schematic diagram showing the definition of the problem under consideration.

to be described by the Stokes equation and the continuity equation for each phase. Together with the boundary conditions, the problem under consideration is defined by

$$\nabla \cdot U = 0, \tag{1}$$

$$\nabla \cdot \tau = \mathbf{0}, \tag{2}$$

where the stress tensor τ is defined as $\tau = -p\boldsymbol{I} + \eta(\nabla U + \nabla U^T)$, with p representing the pressure and $\boldsymbol{I}$ the identity tensor. The boundary conditions are:

$$U = U^{\infty} \quad \text{as} \quad x \to \infty,$$

$$U = -hG\boldsymbol{e}_2$$

at the wall for a simple shear flow G. At the droplet surface, continuity of velocity is required,

$$U^{ext} = U^{int}.$$

The discontinuity of the normal stress component at the droplet interface is determined by the surface tension and local geometry

$$(\tau \cdot \boldsymbol{n})^{ext} - (\tau \cdot \boldsymbol{n})^{int} = \sigma \boldsymbol{n} \nabla \cdot \boldsymbol{n},$$

with $\boldsymbol{n}$ the outward normal of the droplet and $\nabla \cdot \boldsymbol{n}$ twice the mean surface curvature.

In order to solve the Stokes equation with the proper boundary conditions for the fluid droplet, we make use of the boundary integral method, which has already been successfully applied to similar problems (Pozrikidis 1992; Uijttewaal *et al.* 1993). This method has the advantage that the velocities at the interface of the droplet are found by calculating an integral over the droplet surface only. This is especially suitable to a problem where the surface has no fixed geometry and the geometry is of greater interest than the complete flow field inside and outside the droplet. In the boundary integral representation, the k-component of the dimensionless interfacial velocity is given by

$$U_k = \frac{2C}{1+\lambda} U_k^{\infty} - \frac{2(1-\lambda)}{1+\lambda} \int_S K_{ijk}(\boldsymbol{r})\, U_i(\boldsymbol{y})\, n_j(\boldsymbol{y})\, \mathrm{d}S(\boldsymbol{y})$$

$$- \frac{1}{4\pi(\lambda+1)} \int_S J_{jk}(\boldsymbol{r})\, n_j(\boldsymbol{y})\, \nabla \cdot \boldsymbol{n}\, \mathrm{d}S(\boldsymbol{y}), \tag{3}$$

where λ denotes the ratio of the droplet and medium viscosity η_i/η_e, $C = \eta_e Ga/\sigma$ is the dimensionless capillary number and U^{∞} the imposed flow at $x \to \infty$. The Green's function tensor $\boldsymbol{J}$ and the stress tensor $\boldsymbol{K}$ were derived by Blake (1971) for a domain

bounded by a plane wall in terms of an image system (see also Pozrikidis 1990). The integral equation has a unique continuous solution for $0 < \lambda < \infty$, as was proved by Power (1987). Equation (3) becomes explicit for the case $\lambda = 1$ giving rise to a drastic reduction in computational effort (Uijttewaal *et al.* 1993).

3. Numerical solution method

In contrast to other comparable problems concerning droplet motion with or without a plane wall, the integrals of (3) cannot be reduced to one dimension. The only reduction in the computations lies in the remaining plane symmetry in the (x_2, x_3)-plane. In order to solve (3) numerically, the surface of the droplet was discretized with triangles. Evaluation of the surface properties like curvatures and normal vectors was performed at the triangle vertices. We therefore fitted locally a second-order surface with six free coefficients α_m, given by

$$\alpha_1 x_1^2 + \alpha_2 x_2^2 + \alpha_3 x_3^2 + \alpha_4 x_1 x_2 + \alpha_5 x_1 x_3 + \alpha_6 x_2 x_3 = 1, \tag{4}$$

through one marker point (x_1, x_2, x_3) and five of its nearest neighbours. From this surface, the normal vector and curvature as required in (3) were easily obtained by determining the first- and second-order gradients from (4). It is clear that for ellipsoidal droplets these fits are exact while for deviations from the ellipsoidal shape the approximation is still accurate owing to the free choice of the coefficients at each separate grid point.

Both kernels $\boldsymbol{J}$ and $\boldsymbol{K}$ in (3) are singular. The former is integrable and was solved with a four-node Euler–Legendre quadrature. The latter can be solved by making use of the special properties of the principal value integral (Ladyzhenskaya 1969; Pozrikidis 1990).

After integrating (3) a set of linear equations is obtained that can be solved either by matrix inversion (Rallison & Acrivos 1978) or by an iterative method (Pozrikidis 1990). We have chosen the latter method because of its efficiency in arithmetic operations and guaranteed convergence.

With the solution for the surface velocities thus obtained, the positions of the marker points on the droplet are advanced using the modified Euler method. With the evolution of time the marker points become unevenly distributed, especially in cases of high deformation. In order to obtain a numerically stable and sufficiently accurate scheme for these cases, the points are redistributed after each time step. The approximation of a continuous interface of the droplet according to (4) is used here again. The marker points are displaced tangentially within this surface so that the redistribution has effect neither on the shape nor on the volume of the drop.

In the case with a wall present, an initially spherical droplet was allowed to deform and migrate away from the wall. The lateral and slip velocities were then determined after a sufficient period of time when the transient motion had vanished. This is in contrast with Uijttewaal *et al.* (1993) where the droplet was kept at a fixed position during the calculations. For $\lambda = 1$ we observed hardly any difference between the migration velocities obtained for the 'free' and the 'fixed' particles. This was because the time needed for the droplet to deform to a steady shape was small compared to the time needed for the droplet to migrate away from the wall significantly. Therefore the droplet shape could be considered as quasi-steady. With $\lambda > 1$, however, the deformation time increases while the migration time remains the same, making the cases of a free and a fixed particle different. Since the free droplet represents reality best, we preferred this approach in the present calculations.

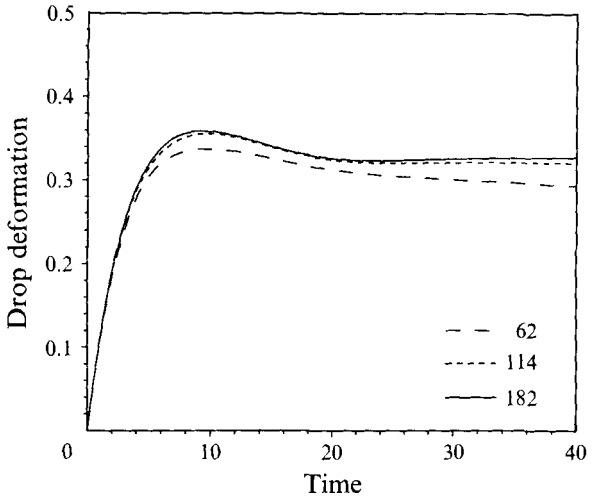

FIGURE 2. Computations on drop deformation with various numbers of grid points for $\lambda = 3.6, C = 0.5$.

In order to assess the accuracy of the results we performed calculations varying the number of grid points as well as the time discretization. In figure 2 we depict the time-dependent deformation of a droplet with $\lambda = 3.6$ and $C = 0.5$ calculated with 62, 114 and 182 grid points. The difference between the three curves originates mainly from the changes in the droplet volume, which are largest with 62 grid points. The time-step size has an effect on the stability of the numerical scheme especially with highly deformed droplets. When it is sufficiently small, typically < 0.1, the time discretization merely affects the droplet volume. We therefore consider the extent to which mass is conserved (equation (1)) as an important criterion for the accuracy of the computations. The volume of the droplet as well as its centre of gravity could easily be calculated by means of Green's surface integral at each time step. During the calculations with 182 grid points the volume changes could be kept to within 0.5% per unit of dimensionless time at $\lambda = 0.1$, and down to 0.03% at $\lambda = 10$.

4. Results and discussion

4.1. *Motion in the absence of a wall*

4.1.1. *Deformation, orientation and circulation*

We first consider the steady deformation of the fluid droplet in linear shear flow in the absence of a wall. The evolution of the drop is governed by the two physical parameters C and λ. The ranges of these parameters are limited by (i) physical properties like droplet burst and (ii) numerical limitations like the slow convergence of the iterative matrix solving procedure at both very small and very large values of λ, and the above-mentioned volume changes at very small values of λ.

We consider an initially spherical drop subjected to a sudden shear flow at $T = 0$ and follow the evolution of the droplet deformation in time until a steady state is reached. The deformation of the droplet, figure 3, is according to Taylor (1934) defined as $D = (L-B)/(L+B)$, where L is the longest and B the shortest axis in the equatorial plane. It follows from figure 3 that for viscosity ratios smaller than 2 and for $C < 0.4$, the deformation is approximately proportional to the capillary number, with a constant only slightly depending on λ. The slight decline of the slope with λ decreasing from 1.0

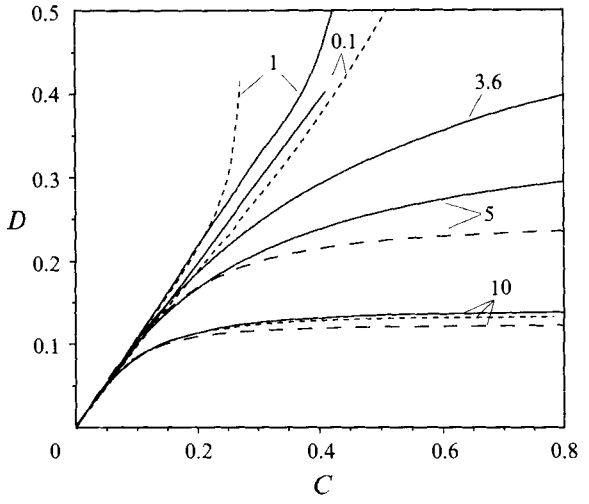

FIGURE 3. Droplet deformation D versus capillary number C calculated for various values of λ compared with Cox's (1969) model (——) for $\lambda = 5, 10$ and quadratic theory of Barthès-Biesel & Acrivos (1973) (----) for $\lambda = 0.1, 1, 10$.

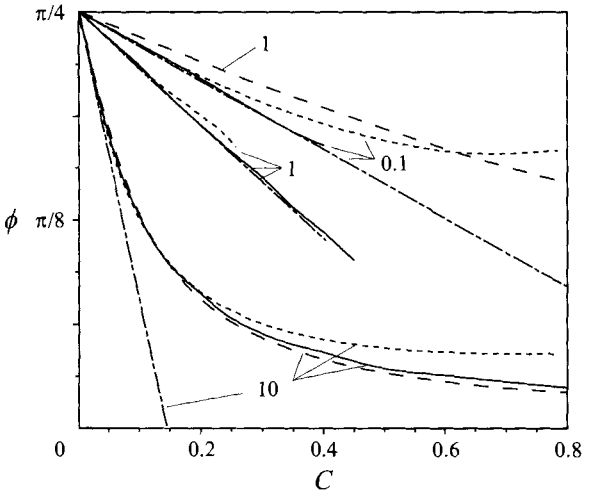

FIGURE 4. Droplet orientation ϕ versus C calculated for various values of λ, compared to typical results from the models of Cox (1969) (——), Cerf (1951) (—·—·) and Barthès-Biesel & Acrivos (1973) (----).

to 0.1 is in accordance with the small-deformation theories of Taylor (1934) and Cox (1969). At higher values of λ the deformation still increases with C but at a smaller rate at higher C. At the highest values of $\lambda(> 10)$ the deformation finally becomes independent of C. The slope of the deformation curves reveals good agreement with the analytical models at low values of λ and C, whereas in the range $2 < \lambda < 10$ deviations are large, especially at high C. A comparison has been made with the quadratic model of Barthès-Biesel & Acrivos (1973) for $\lambda = 0.1$, 1.0 and 10 (dotted lines in figure 3) showing a good qualitative agreement for all values of λ. Quantitative agreement is pretty good for $\lambda = 10$, even better than the model of Cox (1969).

The orientation angle ϕ, defined as the angle subtended by the x_2-axis and the major axis of the deformed droplet, is presented in figure 4. It can be seen that at low C the

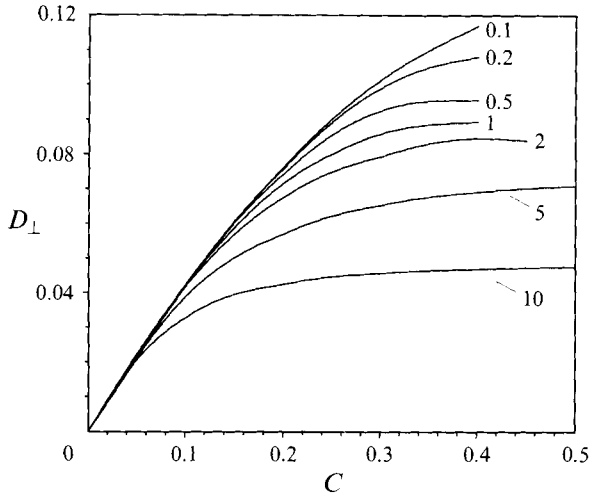

FIGURE 5. Droplet deformation in the plane perpendicular to the longest axis of deformation L, $D_\perp$ versus C for various values of λ.

orientation is proportional to C, while the slope depends strongly on λ. At high C and high λ the proportionality is less prominent and the curves tend to the limiting orientation of complete alignment with the streamlines, i.e. $\phi = 0$. Comparison with the models of Cerf (1951) (with a correction by Roscoe 1967), and Cox (1969) shows that Cox's model is only applicable for large λ whereas Cerf's model gives a good approximation for $\lambda < 1$. It should be mentioned that Cerf derived his model for elastic spheres but concluded that it should be also applicable to the case of fluid drops. Again the quadratic theory of Barthès-Biesel & Acrivos (1973) gives a good qualitative description of the droplet orientation over the whole range of λ, and is quantitatively correct for $C < 0.2$.

An interesting property, so far disregarded in both experiments and theory, is the deviation from rotational symmetry in the shape of the particle with respect to the major axis of deformation. Figure 5 presents the deformation $D_\perp$ perpendicular to the longest axis of deformation. A positive value of $D_\perp$ means that the droplet is slightly extended in the x_1-direction. (For rotational symmetry this deformation index should be zero.) The extensional component of the linear shear flow finds its most prominent expression in large droplet deformation and orientation close to $\pi/4$ with droplets of low viscosity (figures 3, 4). The compression force in the (x_2, x_3)-plane acting on the short axis of the droplet will therefore lead to an increasing amplitude of $D_\perp$ with decreasing λ.

As a consequence of the vorticty of the shear flow, the droplet exhibits in addition to deformation a rotational motion. This means that the fluid inside the droplet circulates with a certain periodicity. The characteristic property for the circulation of the droplet, known as the circulation number, is defined as $M = TC/4\pi$, where T is the dimensionless time required for a material point in the equatorial plane to make a closed loop around the circumference of the droplet. The lowest possible value of $M = 1$, indicating the fastest rotation, represents a circulation corresponding to the vorticity of the shear flow. This limiting case applies for a rigid sphere. It is known from the work of Rumscheidt & Mason (1961*b*) that the analytical models give only reasonable predictions for $\lambda \geqslant 1$ and $D \to 0$. Furthermore, Rumscheidt & Mason (1961*a*) have demonstrated the dramatic effects of minute traces of surface-active

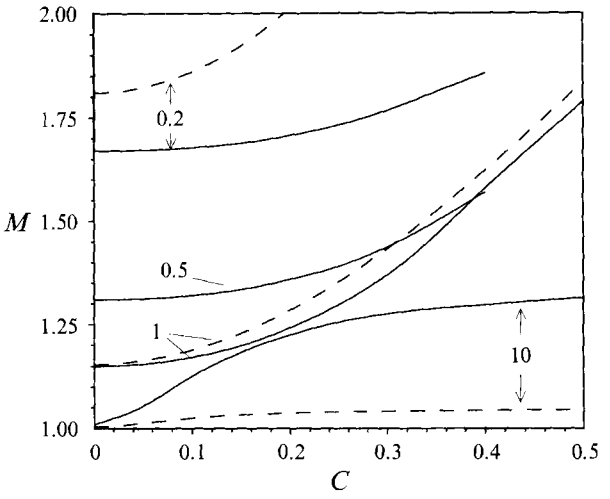

FIGURE 6. Droplet circulation M versus C for various values of λ. Dashed lines according to the model of Torza *et al.* (1972).

impurities on drop circulation, making high demands on the experimental procedure. In our calculations M could be determined at any time step by integrating the reciprocal tangential velocities around the circumference in the equatorial plane. Figure 6 shows the circulation number *vs.* C at various values of λ. As expected for the limit $C \to 0$ and $\lambda \to \infty$ the rotational motion resembles that of a rigid sphere. At $\lambda = 1$ the agreement between calculations (solid curves) and analytical predictions (dashed curves) is good. Only when C becomes large does the resemblance diminish. For $\lambda < 1$ the circulation number is always overestimated by the analytical model, becoming even worse for large C. The theoretical curve for $\lambda = 10$ on the other hand appears correct only for $C = 0$. For larger C the agreement is poor again.

An example will now be given to illustrate the characteristic differences between the results from our model, analytical theories of Taylor (1934), Cox (1969), Barthès-Biesel & Acrivos (1973) and experiments of Torza *et al.* (1972), for the case of stationary deformation and orientation. Figure 7(*a*) shows the deformation versus C for $\lambda = 3.6$. The correspondence between our calculations and the experimental data is good whereas the analytical models show large deviations when C becomes large. When comparing the theoretical curves of figure 7(*a*) with our numerical results it is instructive to see how for $C \mid 0$ all curves coincide while for increasing capillary numbers the models successively start to deviate. First, the model of Taylor, derived for small values of λ and C, then followed by Cox, a small-deformation theory of first order in C. The model of Barthès-Biesel & Acrivos (1973) of second order in C finally start to deviate as a result of breakup phenomena. Although the general shape of the experimental curve is predicted reasonably by the model of Barthès-Biesel & Acrivos (1973), their model predicts droplet burst at $C \approx 0.5$ while the experiments and our calculations show a stationary deformation up to $C \approx 0.8$.

The orientation of the droplet is shown in figure 7(*b*) where the analytical models of Cerf (1951), Cox (1969) and Barthès-Biesel & Acrivos (1973) are also depicted. Again the calculations agree fairly well with the experiment though deviations are still present.

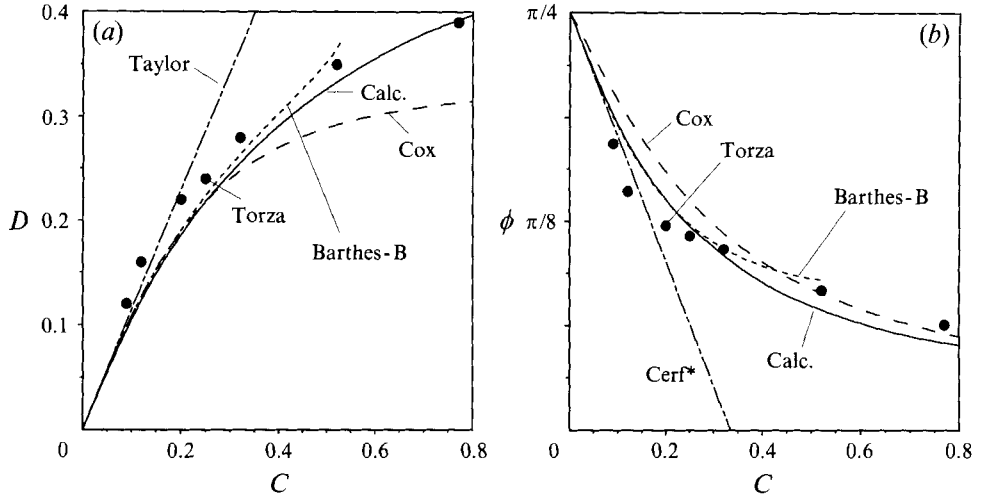

FIGURE 7. Comparison of computations (solid line) with experimental data ● (Torza *et al.* 1972) $\lambda = 3.6$ and models of Taylor (1934), Cox (1969), Cerf (1951) and Barthès-Biesel & Acrivos (1973) (dashed lines): (*a*) deformation, (*b*) orientation.

λ	C_{cr}(exp)	C_{cr}(sim)
0.5	0.4	0.5
1.0	0.5	0.6
2.0	0.8	1.3
3.3	5.2	3.5

TABLE 1. Critical capillary numbers for droplet stability. Simulations compared with experiments of de Bruin (1989)

4.1.2. *Droplet stability*

In order to investigate whether our model is suitable for predicting droplet breakup we compared the maximum capillary number yielding a stable droplet deformation with experimental data from de Bruin (1989), for four different viscosity ratios. In determining the stability of the droplet we could not distinguish between a physical breakup process and numerical instabilities resulting from the highly deformed mesh. The results obtained should therefore be interpreted as a conservative estimate. Table 1 shows a reasonable agreement between numerically and experimentally obtained critical capillary numbers. Only for the viscosity ratio of 3.3 is the discrepancy rather large. It should however be mentioned that the critical capillary number for $3 < \lambda < 4$ shows a very steep increase from about 3 up to 100. It is known from experiments (Torza *et al.* 1972; de Bruin 1989) that beyond $\lambda = 4$ the droplet cannot be broken up by using a simple shear flow. The critical capillary numbers obtained with these simulations are reasonably confirmed by the experimental data of de Bruin (1989) and Torza *et al.* (1972) while, for example, the second-order model of Barthès-Biesel & Acrivos (1973) consistently underestimates these values. Although our data on droplet breakup are of limited accuracy they indicate theoretical evidence of droplet breakup at capillary numbers that are significantly higher than those predicted by a second-order breakup model, at least in the range considered here.

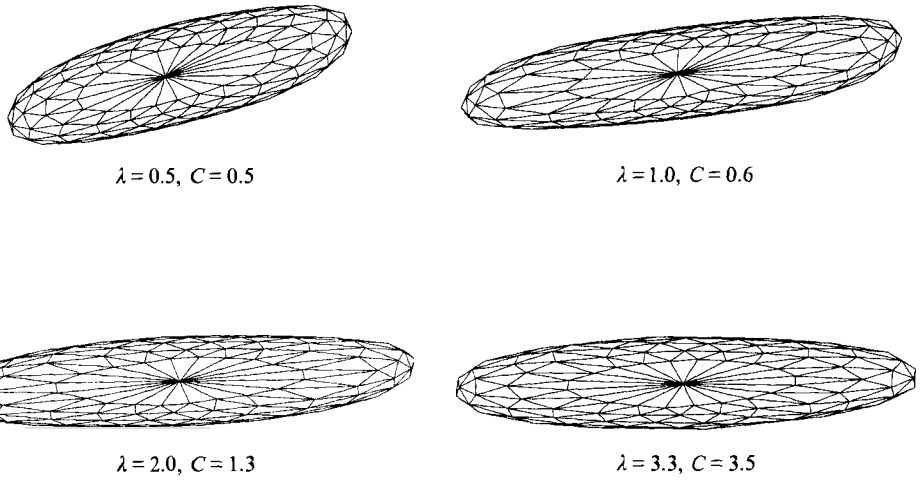

FIGURE 8. Droplet shapes at capillary numbers near the critical breakup values (table 1).

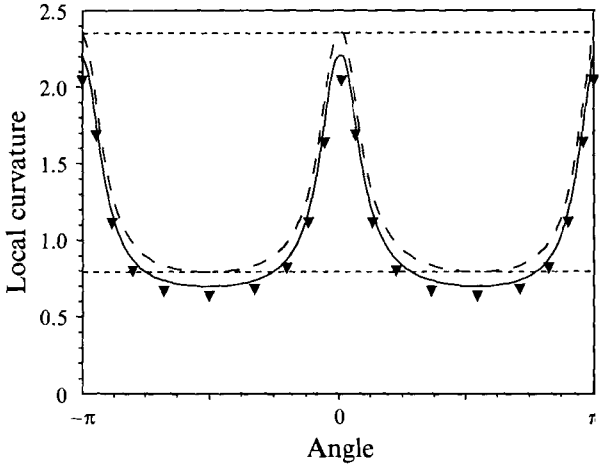

FIGURE 9. Local curvature in the plane of symmetry for a simulated droplet ($\lambda = 1.0, C = 0.3$) (symbols) compared with the curvature along an axisymmetric ellipsoid (dashed line) and an ellipsoid with three different principal axes in agreement with the droplet shape (solid line). Horizontal dotted lines are the analytically obtained minimum and maximum curvatures for the axisymmetrical ellipsoid.

For a closer look at droplet deformation, we depict in figure 8 the shapes of the droplets close to breaking up, corresponding to table 1. We see that despite small disturbances of the mesh the particle surface is rather smooth. A more accurate prediction of droplet breakup and shape requires a surface discretization that is more suitable and more stable for highly deformed drops. However, as breakup phenomena are not our main interest, we made no further attempts to improve our model for that purpose.

In order to demonstrate how a droplet shape deviates from an ellipsoid with the same deformation we compared in figure 9 the mean surface curvature $\nabla \cdot \boldsymbol{n}/2$ at the grid points along the circumference in the plane of symmetry. The symbols represent the values obtained by simulating a droplet with $\lambda = 1$ and $C = 0.3$. With that same algorithm the curvature of an axisymmetrical ellipsoid with the same deformation was

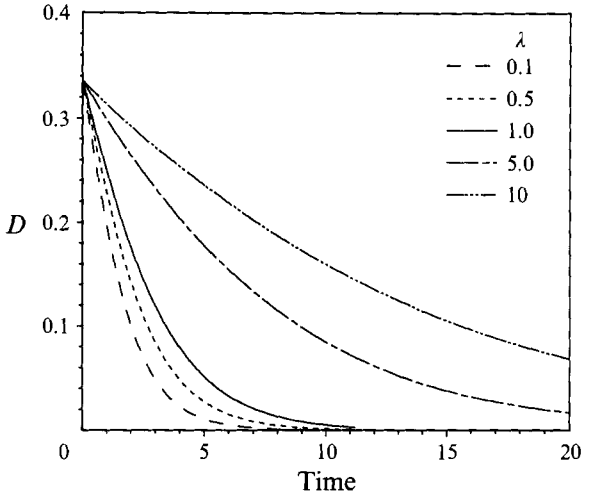

FIGURE 10. Relaxation of an initially ellipsoidal-shaped droplet of $4\pi/3$ volume with axis ratio 1:1:2 in an otherwise quiescent fluid calculated for various viscosity ratios.

computed and is depicted as a dashed line. The maximum and minimum values of the ellipsoid curvature can easily be calculated analytically (horizontal dotted lines) and coincide perfectly with the values obtained with our code. In the same graph we depict the curvature along an ellipsoid where the deformation in the perpendicular (x_1-) direction (like in figure 5) has been taken into account (solid line). The fact that the curvature found for the axisymmetrical ellipsoid is always smaller than that of the ellipsoid with three different axes but with the same volume can be illustrated by considering that the perpendicular deformation lowers the curvature in the x_1-direction. Obviously the droplet is able to reduce the curvature in the plane of symmetry even slightly more.

4.1.3. *Time-dependent deformation*

A model giving a reasonable qualitative description of the time-dependent deformation was derived by Cox (1969). This model predicted the interesting phenomenon called 'wobbling', originating from the differences in time scale between deformation of the drop and rotation of the applied external flow field. It was pointed out by him and later confirmed by Rallison (1980) that his model for the time-dependent deformation applies only in the limit of small $\mathrm{d}D/\mathrm{d}t$ and large λ. Experimental data on time-dependent deformation are scarce so models can only be compared with the studies of Torza *et al.* (1972) and de Bruin (1989).

A characteristic measure for the evolution of time-dependent behaviour is the relaxation time of an initially ellipsoidal droplet in an otherwise quiescent fluid, i.e. $C = 0$. Figure 10 shows the reduction of the deformation of an ellipsoidal drop with axis ratios 1:1:2 ($D = 0.33, D_\perp = 0$) computed for various viscosity ratios. It is clear from figure 10 that the relaxation time is strongly related to λ especially when λ is large. When the drop viscosity is low the relaxation time tends to a constant value. This can be understood by considering the relaxation time always to be dominated by the most viscous of the two fluids when time has been made dimensionless using the interfacial tension and the viscosity of the continuous phase η_e.

For the case of an initially spherical drop instantaneously subjected to a constant shear flow, the time required for the drop to obtain a stationary deformation will be

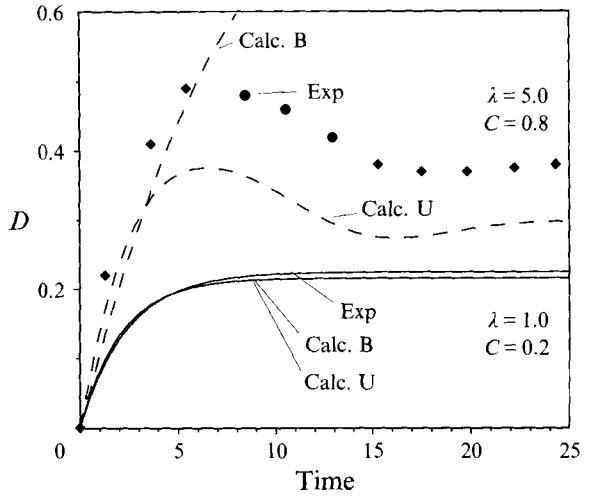

FIGURE 11. Simulated transient droplet deformation (Calc. U.) on instantaneously applied shear flow, compared with experimental (exp.) and numerical (Calc. B.) work of de Bruin (1989).

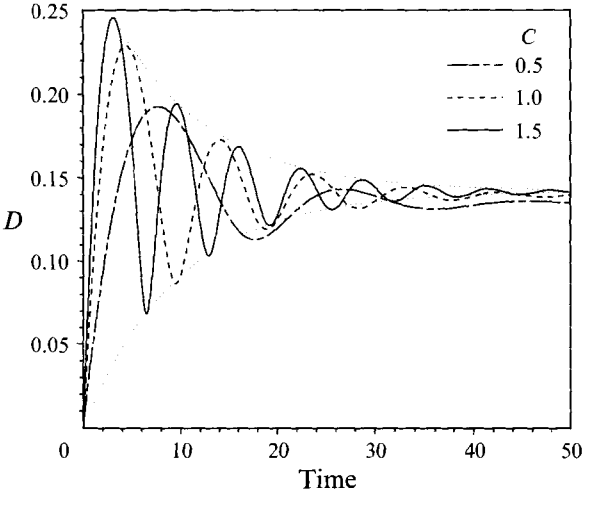

FIGURE 12. Damped wobbling of a droplet $\lambda = 10$ for three capillary numbers. Dotted lines indicate exponential decaying oscillation.

comparable to the relaxation time. Figure 11 shows experimental and numerical data of de Bruin (1989) on the evolution of droplet deformation in time together with our calculations, for $C = 0.8$ and $\lambda = 5$. Our calculations predict an approximately correct evolution in time but with an underestimated amplitude of deformation. Later we will find the same discrepancies with an even larger value of $\lambda = 25$. The numerical calculations of de Bruin (1989) are more difficult to interpret and seem to indicate droplet burst after only 12 units of time. For the case $C = 0.2$ and $\lambda = 1$ both numerical models coincide whereas the experiments give only a slightly higher value for the final deformation.

An interesting phenomenon typical for high viscosity ratios is the small overshoot of the deformation. This 'wobbling' phenomenon of the droplet is depicted in more detail in figure 12 for $\lambda = 10$ at different capillary numbers. It can easily be seen that the

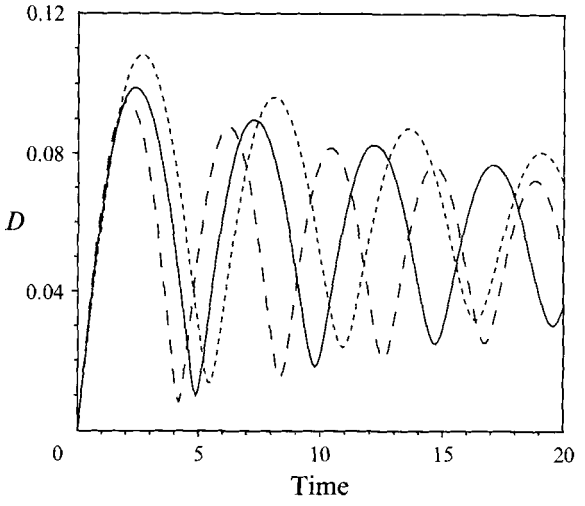

FIGURE 13. Transient drop deformation, calculations for $\lambda = 25$ and $C = 1.5$ (——) and experiments of Torza *et al.* (1972) (----) and theory of Cox (1969) (– – –). Calculations coincide with the model according to Rallison (1980).

exponential damping (dotted lines) of the oscillations is in effect constant irrespective of C. The wobbling frequency however is proportional to C within 2%. At larger values of λ the effects are more pronounced as is shown in figure 13 for $\lambda = 25$ and $C = 1.5$. Again our results are compared with the model of Cox and in addition with the experiments of Torza *et al.* (1972). Although qualitative agreement is good, even the better prediction by our model and the virtually coinciding results of Rallison (1980) do not agree with the experimental data. A possible explanation for the discrepancy might stem from experimental imperfections. As was stated in §4.1.1, Rumscheidt & Mason (1961 *a*) found that the circulation was always hindered by the presence of small traces of impurities. The change of the circulation will affect the deformation of the droplet as well as the wobbling time constant during transient motion. Otherwise it is likely that the assumptions made in our model, such as the Newtonian viscosities of the fluids, the linearity of the flow field and, not least, the absence of inertia, do not completely cover experimental conditions.

4.2. *Influence of a plane wall on droplet motion*

The relative velocity of the droplet with respect to the undisturbed flow field has a component parallel with the wall, for deformable as well as rigid particles, and a component perpendicular to the wall, only present for deformable particles in the absence of inertia. As reported in Uijttewaal *et al.* (1993), the migration velocities are highly dependent on drop deformation and orientation. In the previous subsection we showed that the analytical models for drop deformation are of limited value. It might be expected that the analytical models for drop migration, which are based on the deformation models too, also have their limitations. After properly non-dimensionalizing, the lateral migration velocity, as derived by Chan & Leal (1979)

$$\frac{U_{lat.C.L.}}{(Ca/h)^2} = \frac{16+19\lambda}{16+16\lambda}\frac{3(54\lambda^2+97\lambda+54)}{280(1+\lambda)^2}, \tag{5}$$

can be compared with our calculations. An example of the determination of the lateral

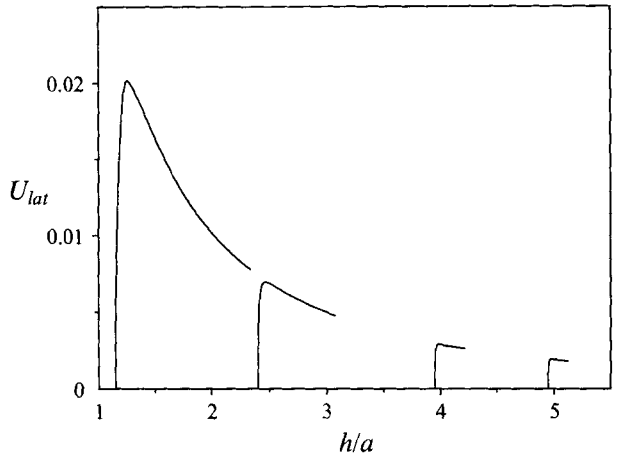

FIGURE 14. Evolution of lateral velocity at four different starting positions of an initially undeformed droplet, with $C = 0.3, \lambda = 0.5$.

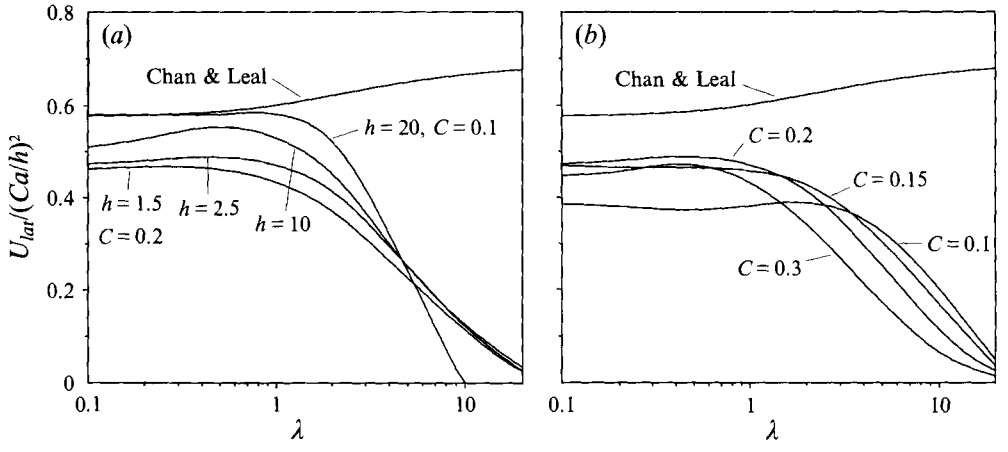

FIGURE 15. $U_{lat}/(Ca/h)^2$ versus λ for (*a*) $h = 1.5$, 2.5 and 10 with $C = 0.2$ and (*b*) $C = 0.1$, 0.15, 0.2 and 0.3 with $h = 2.5$ compared with the model of Chan & Leal (1979). In (*a*) the curve with $h = 20$ and $C = 0.1$ shows correspondence with the model for small λ.

migration velocity is shown in figure 14 for $\lambda = 0.5, C = 0.3$ for different starting positions. Starting with a spherical droplet at a position h/a the droplet deforms and the migration velocity rapidly increases. As the droplet obtains a steady shape the migration velocity starts to decrease as a result of the increasing distance between the particle and the wall. It is therefore necessary to determine the lateral migration velocity from these curves a sufficient period of time after the maximum in the curve. For proper comparison with the model of Chan & Leal we divided the calculated velocity by $(Ca/h)^2$ making the expression depend exclusively on λ. In figure 15(*a*) this factor is shown for $C = 0.2$ and for wall distances $h/a = 1.5, 2.5, 10$ respectively, revealing its slight dependency on h. The depicted theoretical curve according to Chan & Leal (1979) shows that the lateral velocity is always overestimated by their model. It becomes clear, especially at small wall distances, that their postulate of a remote wall is violated, making the model less accurate in these cases. In order to verify the consistency of our model we depict in addition the lateral migration velocity calculated

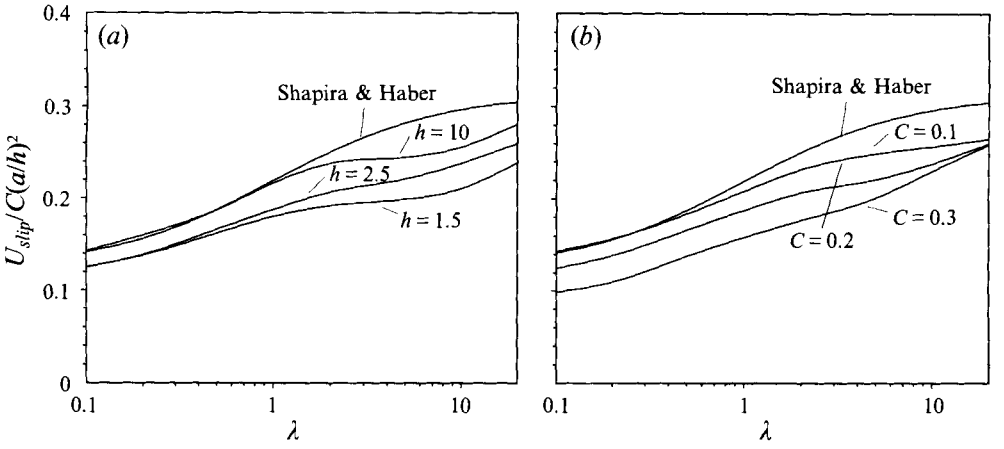

FIGURE 16. $U_{slip}/(a/h)^2 C$ versus λ for (*a*) $h = 1.5$, 2.5 and 10 with $C = 0.2$ and (*b*) $C = 0.1$, 0.2 and 0.3 with $h = 2.5$ compared with the theory of Shapira & Haber (1990).

with $h = 20$ and $C = 0.1$. For this case the agreement with the Chan & Leal model is pretty good for $\lambda < 1$. By assuming a droplet shape according to Taylor (1934) and a $\pi/4$-orientation their analysis clearly fails for $\lambda > 1$. In the limit $\lambda \to \infty$ the droplet will behave like a rigid sphere and will therefore not migrate with respect to the wall. This finds expression in the decline of U_{lat} with increasing viscosity ratio. In contrast with this, simulations of Kennedy *et al.* (1994) show migration velocities slightly smaller than the Chan & Leal model for $\lambda = 1$ and $C = 0.159$, whereas with $\lambda = 6.4$ they found values at least three times the Chan & Leal model.

Calculations were also performed for various values of C as depicted in figure 15(*b*) with $h = 2.5$. It can be seen that the factor $U_{lat}/(Ca/h)^2$ is not fully independent of C. Because the proportionality of D with C is better maintained at small C (figure 3) the curves start to decline at higher values of λ in these cases. Data obtained for $\lambda < 1$ are more difficult to interpret. The left part of figure 15(*b*) shows that at $C \approx 0.2$ the factor is maximum over a substantial range of λ. Obviously, at a distance $h = 2.5$ the wall cannot be considered as remote and higher-order effects like excess deformation and alignment due to the presence of the wall become appreciable, affecting the lateral migration velocity (Uijttewaal *et al.* 1993).

Data obtained for the slip velocity can be treated similarly. Shapira & Haber (1990) derived for the velocity difference between the undisturbed fluid flow and the particle velocity

$$\frac{U_{slip\,S.H.}}{C(a/h)^2} = \frac{1+2.5\lambda}{8(1+\lambda)}. \tag{6}$$

In the limit of $\lambda \to \infty$, (6) is the same as the result obtained by Goldman, Cox & Brenner (1967) for rigid spheres. Figure 16(*a*) shows a comparison of (6) with computations. Again the analytical model gives larger values than the numerical results especially at small wall distances. For $h = 10$ the agreement is very good, showing only small deviations for $\lambda > 2$. It should be noted that Shapira & Haber (1990) did not take into account that for large λ the longest axis of the deformed droplet is aligned almost parallel to the wall (figure 4) leading to a small reduction of the slip velocity. For still larger λ the slopes of the curves show a slight increase, indicating that the droplet motion for the limit $\lambda \to \infty$ resembles that of a rigid sphere. The effect of the capillary

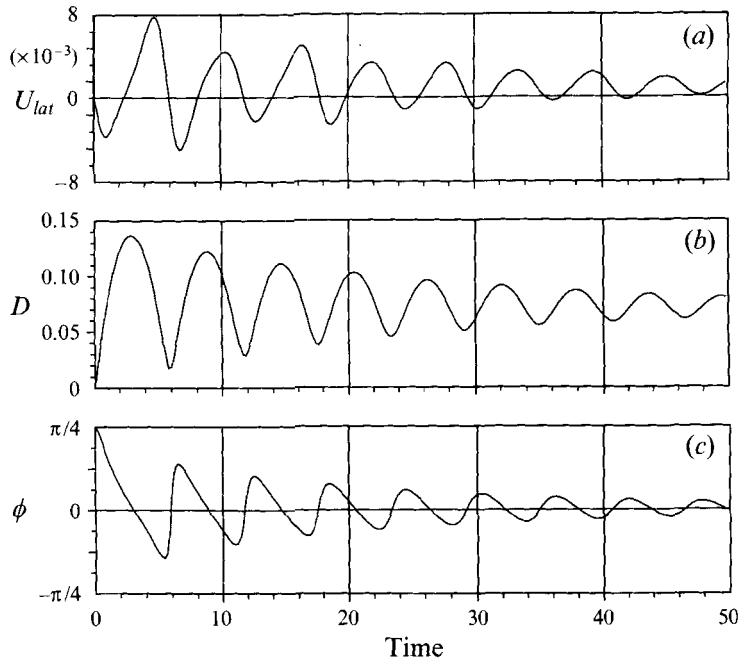

FIGURE 17. The effect of wobbling motion on lateral migration for $\lambda = 25$, $C = 1.5$ and $h \approx 1.52$: (*a*) migration velocity, (*b*) deformation and (*c*) orientation.

number on deviations from the analytical model for $h = 2.5$ is shown in figure 16(*b*). At higher values of C the assumptions of small deformation and fixed $\pi/4$-orientation cannot be met, leading to a reduction of the slip velocity.

Recently Smart & Leighton (1991) reported measurements on the lateral drift of a droplet ($\lambda = 0.08$) in a Couette device and compared their experimental results with a model almost identical with that of Chan & Leal (1979). Although their experiments confirmed the $(Ca/h)^2$ dependency of U_{lat}, the experimentally found lateral velocities were always larger (by up to 50%) than predicted by their model. This is in contrast with the results obtained from figures 15(*a*) and 15(*b*). As stated in Uijttewaal *et al.* (1993) the discrepancies found might be imputed to a small curvature in the flow field of their Couette device with an aspect ratio (gap width divided by average radius) of 0.17. The influence of this curvature is clearly demonstrated in their figure 3 where droplets migrate away from the outer Couette cylinder and find an equilibrium position significantly beyond the centre of the gap nearer to the inner cylinder (see also Chan & Leal 1981).

4.2.1. *Wobbling and migration*

It is clear that the amplitudes of the lateral and slip velocities as presented above are highly sensitive to fluctuations in droplet deformation and orientation. It is therefore interesting to observe how the time-dependent lateral migration of a wobbling droplet depends on variations in deformation and orientation. In figure 17(*a–c*) we depicted the transient motion of a wobbling droplet with $\lambda = 25$, $C = 1.5$ and $h = 1.5$. Owing to the wobble motion the lateral velocity varies with the same periodicity as the deformation but with a phase difference of nearly $\pi/2$. The phase difference with the orientation is π. With lower viscosity ratios the damping of the oscillations is stronger

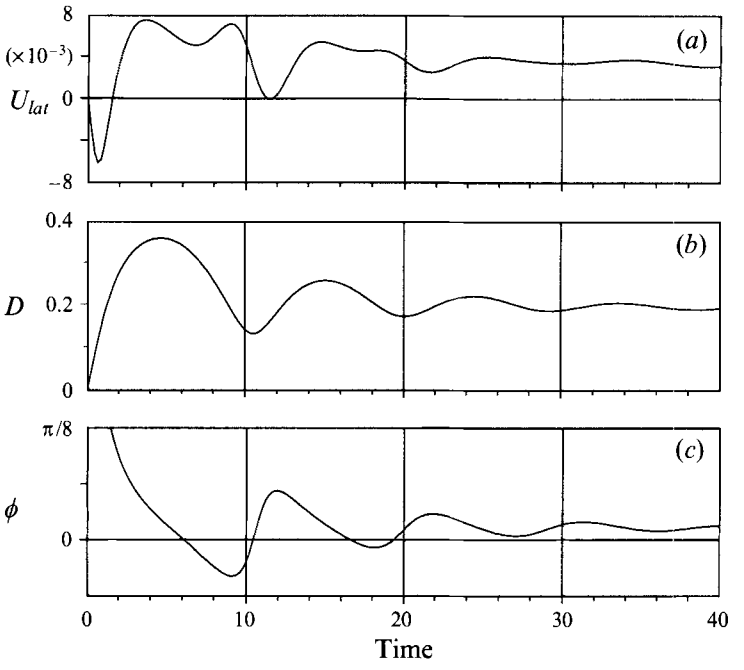

FIGURE 18. The effect of wobbling motion on lateral migration for $\lambda = 10$, $C = 1.5$ and $h \approx 1.55$: (*a*) migration velocity, (*b*) deformation and (*c*) orientation.

and the phase relations become less clear as is shown in figure 18(*a–c*) for $\lambda = 10$. This indicates that the lateral migration is not related to the orientation or deformation of the droplet in a simple way. Furthermore it is interesting to note that in both cases the droplet initially migrates towards the wall. This behaviour, only observed with $\lambda > 2$, was always transient. During stationary motion we never found migration towards the wall.

5. Concluding remarks

In this paper we have shown the results of numerical simulations of droplet motion in Stokes flow. It was demonstrated how deformation, orientation, and circulation of the droplet was affected by the externally applied simple shear flow and to what extent the existing analytical models are applicable. The boundary integral technique we used to solve the problem is well suited for applying to other types of flow. Comparing our results with small-deformation theories of first- and second-order accuracy in C reveals the limitations of those models. With high capillary numbers ($C > 0.3$) and intermediate viscosity ratios ($2 < \lambda < 10$) in particular, the assumption of small deformation no longer holds and the agreement with our calculations and experimental data successively fails with increasing C. We observe similar discrepancies for droplet orientation. Cox's model appears valid for highly viscous drops, whereas the predictions of Cerf are in agreement with our calculations for small λ. The second-order model of Barthès-Biesel & Acrivos (1973) gives good predictions for all values of λ, but only with sufficiently small capillary number. For the droplet circulation number we could only find reasonable agreement for the limit $C \to 0$ when $\lambda \geqslant 1$. Another salient finding is the disturbance of the rotational symmetry in the plane

perpendicular to the longest axis of deformation which has never been analysed thus far. Furthermore, the time-dependent deformation, like the wobbling motion, appears to be always slower in our computations than in the theory of Cox (1969). Agreement with experimental data of Torza *et al.* (1972) and the de Bruin (1989) for $\lambda = 25$ and $\lambda = 5$ respectively remained poor although our model comes close.

The lateral and slip migration velocities were also calculated with a wall present. It has been shown that the model of Chan & Leal (1979) for lateral migration yielded higher velocities than our calculations, particularly when the drop was positioned close to the wall. The incorporation of the small-deformation theory which has only limited validity (i.e. $C \to 0, h \to \infty, \lambda \leqslant 1$) into the models on lateral migration is responsible for the dramatic differences, found particularly at high values of λ and C. The large discrepancies between the experimental results of Smart & Leighton (1991) and theories on droplet migration could however not be clarified by our numerical model. The sensitivity to disturbances, and the limited number of experiments on lateral migration of droplets in Couette flow, however, makes it difficult to draw firm conclusions from a comparison with our numerical simulations. Clearly, a combination of extensive experimental research and further numerical investigation is required to obtain a better knowledge on the parameters affecting the migration velocities.

The authors are indebted to drs. J. Wiersma for his contribution in analysing the analytical models, and to prof. dr. R. M. Heethaar for his valuable advice.

REFERENCES

BARTHÈS-BIESEL, D. & ACRIVOS, A. 1973 Deformation and burst of a liquid droplet freely suspended in a linear shear field. *J. Fluid Mech.* **61**, 1–21.

BLAKE, J. R. 1971 A note on the image system for a stokeslet in a no-slip boundary. *Proc. Camb. Phil. Soc.* **70**, 303–310.

BRUIN, R. A. DE 1989 Deformation and breakup of drops in simple shear flows. PhD thesis, Technical University Eindhoven, The Netherlands.

CERF, R. J. 1951 Recherches théoriques et expérimentales sur l'effet Maxwell des solutions de macromolécules déformables. *J. Chim. Phys.* **48**, 59–84.

CHAFFEY, C. E., BRENNER, H. & MASON, S. G. 1965 Particle motions in sheared suspensions XVIII: Wall migration. *Rheol. Acta* **4**, 64–72.

CHAN, P. C.-H. & LEAL, L. G. 1979 The motion of a deformable drop in a second-order fluid. *J. Fluid Mech.* **92**, 131–170.

CHAN, P. C.-H. & LEAL, L. G. 1981 An experimental study of drop migration in shear flow between concentric cylinders. *Intl J. Multiphase Flow* **7**, 83–99.

COX, R. G. 1969 The deformation of a drop in a general time-dependent fluid flow. *J. Fluid Mech.* **37**, 601–623.

FISCHER, T. M. 1987 A boundary integral method for the numerical computation of the forces exerted on a sphere in viscous incompressible flows near a plane wall. *Z. Angew. Math. Phys.* **38**, 339–365.

GOLDMAN, A. J., COX, R. G. & BRENNER, H. 1967 Slow viscous motion of a sphere parallel to a plane wall – II; Couette flow. *Chem. Engng. Sci.* **22**, 653–660.

GOLDSMITH, H. L. & MASON, S. G. 1962 The flow of suspensions through tubes. I. Single spheres, rods, and discs. *J. Colloid Sci.* **17**, 448–476.

KARNIS, A. & MASON, S. G. 1967 Particle motions in sheared suspensions. XXIII. Wall migration of fluid drops. *J. Colloid Interface Sci.* **24**, 164–169.

KENNEDY, M. R., POZRIKIDIS, C. & SKALAK, R. 1994 Motion and deformation of liquid drops, and the rheology of dilute emulsions in simple shear flow. *Computers Fluids* **23**, 251–278.

LADYZHENSKAYA, A. 1969 *Mathematical Theory of Viscous Incompressible Flow*, 2nd edn., pp. 49–67. Gordon & Breach.

POWER, H. 1987 On the Rallison and Acrivos solution for the deformation and burst of a viscous drop in a extensional flow. *J. Fluid Mech.* **185**, 547–550.

POZRIKIDIS, C. 1990 The deformation of a liquid drop moving normal to a plane wall. *J. Fluid Mech.* **215**, 331–363.

POZRIKIDIS, C. 1992 *Boundary Integral and Singularity Methods for Linearized Viscous Flow.* Cambridge University Press.

RALLISON, J. M. 1980 Note on the time-dependent deformation of a viscous drop which is almost spherical. *J. Fluid Mech.* **98**, 625–633.

RALLISON, J. M. 1981 A numerical study of the deformation and burst of a viscous drop in general shear flows. *J. Fluid Mech.* **109**, 465–482.

RALLISON, J. M. 1984 The deformation of small viscous drops and bubbles in shear flows. *Ann. Rev. Fluid Mech.* **16**, 45–66.

RALLISON, J. M. & ACRIVOS, A. 1978 A numerical study of the deformation and burst of a viscous drop in an extensional flow. *J. Fluid Mech.* **89**, 191–200.

ROSCOE, R. 1967 On the rheology of a suspension of viscoelastic spheres in a viscous liquid. *J. Fluid Mech.* **28**, 273–293.

RUMSCHEIDT, F. D. & MASON, S. G. 1961*a* Particle motions in sheared suspensions. XI. Internal circulation in fluid droplets (experimental). *J. Colloid Sci.* **16**, 210–237.

RUMSCHEIDT, F. D. & MASON, S. G. 1961*b* Particle motions in sheared suspensions. XII. Deformation and burst of fluid drops in shear and hyperbolic flow. *J. Colloid Sci.* **16**, 238–261.

SHAPIRA, M. & HABER, S. 1990 Low Reynolds number motion of a droplet in shear flow including wall effects. *Intl J. Multiphase Flow* **16**, 305–321.

SMART, J. R. & LEIGHTON, D. T. 1991 Measurement of the drift of a droplet due to the pressure of a plane. *Phys. Fluids* A **3**, 21–28.

TAYLOR, G. I. 1932 The viscosity of a fluid containing small drops of another fluid. *Proc. R. Soc. Lond.* A **138**, 41–48.

TAYLOR, G. I. 1934 The formation of emulsions in definable fields of flow. *Proc. R. Soc. Lond.* A **146**, 501–523.

TORZA, S., COX, R. G. & MASON, S. G. 1972 Particle motions in sheared suspensions. XXVII. Transient and steady deformation and burst of liquid drops. *J. Colloid Interface Sci.* **38**, 395–411.

UIJTTEWAAL, W. S. J. 1993 On the motion of particles in bounded flows; applications in hemorheology. PhD thesis, University of Utrecht, the Netherlands.

UIJTTEWAAL, W. S. J., NIJHOF, E. J. & HEETHAAR, R. M. 1993 Droplet migration, deformation and orientation in the presence of a plane wall; A numerical study compared with analytical theories. *Phys. Fluids* A **5**, 819–825.

YOUNGREN, G. K. & ACRIVOS, A. 1975 Stokes flow past a particle of arbitrary shape: a numerical method of solution. *J. Fluid Mech.* **69**, 377–403.